ChemComm

Alkali-Induced Crumpling of Ti3C2Tx (MXene) to Form 3D Porous Networks for Sodium Ion Storage

Journal:	*ChemComm*
Manuscript ID	CC-COM-01-2018-000649.R1
Article Type:	Communication

ChemComm

COMMUNICATION

Alkali-Induced Crumpling of $Ti_3C_2T_x$ (MXene) to Form 3D Porous Networks for Sodium Ion Storage

Received 00th January 20xx,
Accepted 00th January 20xx

DOI: 10.1039/x0xx00000x

Di Zhao,[a] Mallory Clites,[a] Guobing Ying, [a] Sankalp Kota,[a] Jie Wang,[b] Varun Natu,[a] Xin Wang,[b] Ekaterina Pomerantseva,[a] Minhua Cao,*[b] and Michel W. Barsoum*[a]

We present a novel strategy for constructing three-dimensional (3D) porous Ti_3C_2Tx (MXene) networks by alkali-induced crumpling of Ti_3C_2Tx nanosheets. The 3D porous Ti_3C_2Tx networks display high capacity and outstanding rate performance as anode materials for sodium-ion batteries.

In 2011, Naguib et al. discovered that by simply immersing Ti_3AlC_2 powders – a MAX phase[1] in HF the 3D structure was converted to 2D. In 2012, they extended the work to several other Al-containing MAX phases, thus discovering a new, large, family of two-dimensional (2D) materials, they labelled MXenes with the general formula $M_{n+1}X_nT_z$, where M is an early transition metal, X is carbon and/or nitrogen, T is a terminal group (-F, -OH, -O, etc.), n =1-3 and z is the number of terminal groups.[2-4] Since then, MXenes have attracted intense research interest for a wide range of applications, including transistors, energy-storage devices and electro-catalysis, due to their unique physicochemical properties and diverse tailorable functionalities.[5-8] Two important properties of MXene, that make them attractive as electrodes for energy storage, are: (1) presence of open space between weakly bonded layers that enables facile insertion and rapid movement of ions, and, (2) high electronic conductivity that ensures fast electron transport during device operation. However, to take advantage of these atomic-level processes the MXene flakes need to be assembled into specially designed nano- or micro-scale electrode architectures whose central aim is to avoid restacking of the 2D flakes.

This work's main goal is to report on a simple and effective method to create crumpled 2D flakes. To prove that these crumpled flakes are useful we carried out an electrochemical study using them as electrodes in Na-ion cells and indeed show that electrodes based on these crumpled sheets outperform their multilayered, ML, counterparts.

It is thus instructive here to review the work carried out to date on MXene-based Na-electrodes. Before doing so, it is important to appreciate that two general strategies used to enhance the electrochemical characteristics of 2D materials are to create an open 3D porous microstructure and/or increase the interlayer spacing, $d_{c/2}$. Note herein the interlayer spacing is designated by $d_{c/2,}$ because it is related to half the c-lattice parameter of the parent MAX phase, viz. the (002) peak. The first ensures that open channels are available to the electrolyte and ions to reach electrochemically active sites. Electrodes, especially those made by filtering colloidal suspensions, suffer from limited electrolyte-accessible surface area due to the restacking of the 2D sheets.[9] A few approaches have been used to tackle this problem. Shah et al. spray dried their colloidal suspension, which resulted in crumpled flakes.[10] Recently, Zhao et al. added micron sized polymer beads to their $Ti_3C_2T_x$ colloidal suspensions and cast films.[11] The films were then heated in an inert atmosphere to burn the polymer spheres resulting in a film in which relatively large spherical pores were present. These films showed a capacity of 320 mAh g^{-1} at 20 mA g^{-1}. Xie et al. used carbon nanotubes, CNTs, to prevent the 2D layers from restacking and reported a stable capacity of ≈ 150 mAh g^{-1}, at 20 mA g^{-1}.[9] Without CNTs, the capacities of filtered films were significantly lower (30 mAh g^{-1} at 20 mA g^{-1}). Quite recently we showed that by adding HCl, and other common acids, to $Ti_3C_2T_x$ suspensions it is possible crumple the flakes. The Na ion capacity was 250 mAh g^{-1} at 20 mA g^{-1}.[12]

Others have tried manipulating $d_{c/2}$ which can be tuned by several methods. For example, by the intercalation of alkali and alkali-earth ions varies $d_{c/2}$ 12-16 Å.[13] The $d_{c/2}$ can also be controlled by intercalating with pre-pillaring agents (e.g. cationic surfactant) and can reach 177 % increase compared with the original spacing. The increased spacing sometimes resulted in better energy storage performance when compared with untreated MXenes.[14]

This work describes a rapid, simple, and effective flocculation approach to fabricate hierarchically porous 3D $Ti_3C_2T_x$ networks composed of crumpled - henceforth referred to as *c*-$Ti_3C_2T_x$ - nanosheets by simply adding alkali M'OH solutions, where M' is Na^+, Li^+, K^+ or tetrabutylammonium, TBA^+, cations to colloidal MXene suspensions. Since the cations end up between the 2D sheets to differentiate them from each other we further designate them as M'-*c*-$Ti_3C_2T_x$. A schematic of the overall process is shown in Fig. 1a.

To produce M'-*c*-$Ti_3C_2T_x$ powders, first a $Ti_3C_2T_x$ colloidal suspension is prepared by etching Ti_3AlC_2 powders in a mixture of LiF and HCl (12 M), followed by delamination through sonication and washing of the powders to the point when the suspension is near neutral. More processing details can be found in in Supporting Information. A typical transmission electron microscope, TEM, image (Fig. S1) shows the $Ti_3C_2T_x$ layers to be mostly single layered,

[a] *Department of Materials Science and Engineering, Drexel University, Philadelphia, PA 19105. E-mail: barsoumw@drexel.edu*
[b] *Key Laboratory of Cluster Science, Ministry of Education of China, Beijing Key Laboratory of Photoelectronic/Electrophotonic Conversion Materials, School of Chemistry and Chemical Engineering, Beijing Institute of Technology, Beijing 100081, P. R. China. E-mail: caomh@bit.edu.cn*
†*Electronic Supplemen*tary Information (ESI) available: Experimental procedure and analysis date. See DOI: 10.1039/x0xx00000x

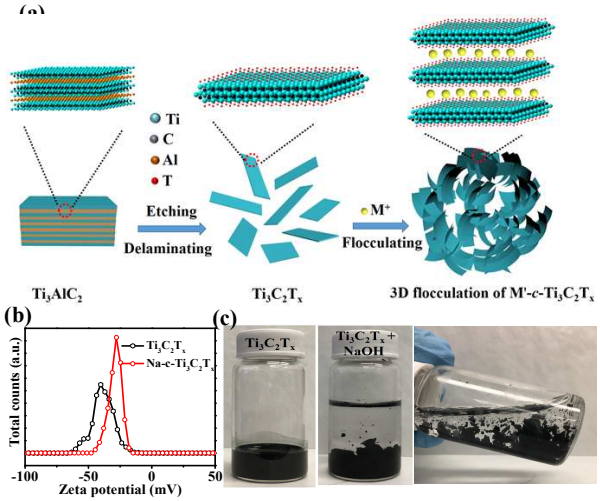

Fig. 1 (a) Schematic of fabrication process for M'-*c*-$Ti_3C_2T_x$ (M^+= Li^+, Na^+, K^+, TBA^+) by flocculation using MOH. (b) Zeta potential of $Ti_3C_2T_x$ and Na-*c*-$Ti_3C_2T_x$ 3D framework at pH ≈ 7. (c) Photographs of $Ti_3C_2T_x$ MXene colloidal suspensions (left), and Na-*c*-$Ti_3C_2T_x$ after flocculation (middle and right).

flat and transparent, confirming their 2D nature. At this stage, it is fairly well established that because of the surface functional groups (e.g., -O, -OH, and -F), the as-prepared $Ti_3C_2T_x$ in water is negatively charged which, in turn, results in stable colloidal suspensions (left panel in Fig. 1c). The zeta potential of the $Ti_3C_2T_x$ and the Na-*c*-$Ti_3C_2T_x$ flakes in water were measured to be ≈ - 40 mV and - 25 mV (Fig. 1b), respectively.

The addition of 1 M M'OH to this stable colloidal suspension induced the flakes to rapidly (< 1 min) flocculate/coagulate/crash out of suspension into what appears to be larger aggregated flakes or flocs. This was true of sodium hydroxide, NaOH (two right panels in Fig. 1c), lithium hydroxide, LiOH, potassium hydroxide, KOH and tetrabutylammonium hydroxide, TBAOH (Fig. S2). To better delineate the NaOH concentrations range over which the flocculation occurs, we systematically added NaOH drops, with different concentrations ranging from 0.5 M to 24 M, into the colloidal suspension. In all cases relatively large flocs – visible to the naked eye - formed readily (Fig. S3). Interestingly, adding 25~28 %, NH_4OH did not result in flocculation (Fig. S4). The reason this is the case is unclear at this time, but could be related to the low concentration of NH_4^+ ions in solution.

Fig. 2a to 2g, respectively, show the XRD patterns of Ti_3AlC_2, $Ti_3C_2T_x$ multilayers, drop cast film, Li-*c*-$Ti_3C_2T_x$, Na-*c*-$Ti_3C_2T_x$, K-*c*-$Ti_3C_2T_x$ and TBA-*c*-$Ti_3C_2T_x$. From these results it is clear that, i) most of the Ti_3AlC_2 is converted to MXene. Note that after etching, some Ti_3AlC_2 peaks (denoted by asterisks) were still present. With the notable exception of the drop cast film (Fig. 2c) all other patterns exhibit a (110) peak at 2θ ≈ 61°. This implies that, in all but the dropcast film, a fraction of the basal planes were *not* parallel to the underlying XRD sample holder, which is consistent with randomly oriented ML particles on the sample holder and/or a crumpled morphology,[15] ii) $d_{c/2}$ immediately after etching, was 14.2 Å (inset in Fig. 2). The same values were obtained for the drop cast films and after flocculation with KOH (inset in Fig. 2). However, after flocculation with LiOH, NaOH or TBAOH, the $d_{c/2}$ values were more than 1 Å larger (inset in Fig. 2). These values are – with the exception of K-*c*-$Ti_3C_2T_x$ – in line with our previous work, where within the range of 15.3 Å and 16 Å, $d_{c/2}$ was more or less,

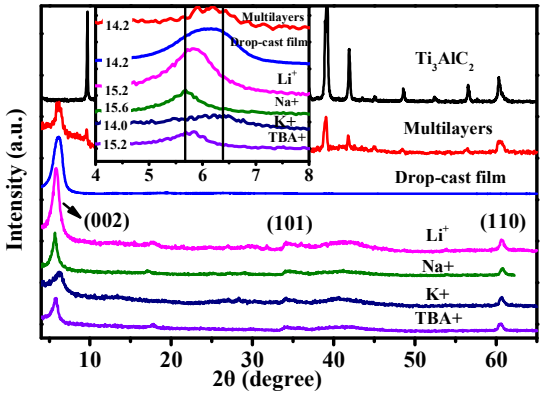

Fig. 2 XRD patterns of, (a) Ti_3AlC_2, (b) $Ti_3C_2T_x$ multilayers, (c) drop cast film, (d) Li-*c*-$Ti_3C_2T_x$, (e) Na-*c*-$Ti_3C_2T_x$, (f) K-*c*-$Ti_3C_2T_x$ and, (g) TBA-*c*-$Ti_3C_2T_x$. Note peak at 2θ ≈ 61° in all but c. Inset shows low angle results. The numbers in inset are the $d_{c/2}$ values calculated from the 002 peak positions. They fall in two groups, separated by ≈ 1 Å. Vertical lines in inset are guides to the eyes.

independent of the nature of the intercalating cation.[13] We also madethe case that these $d_{c/2}$ values corresponded to about two water layers between the $Ti_3C_2T_x$ flakes. It is important to note that the $d_{c/2}$ values of 15.6 Å for Na^+ obtained herein are among the highest values reported for alkali cation intercalated $Ti_3C_2T_x$ (Table S1).[13,16-18]

The most important result of this work is that when the flakes flocculate, they crumple and settle into an interpenetrating, open, foam-like, 3D architecture. SEM images of the open, porous 3D structures obtained when NaOH is used for the flocculation are shown in Fig. 3a. Higher magnification SEM images of the Na-*c*-$Ti_3C_2T_x$ flakes (inset in Fig. 3a) reveal that the porous 3D architecture consists of wrinkled/crumpled, interpenetrating, MXene nanosheets, creating many irregular large pores with diameters between 100−400 nm. Moreover, it is clear that the pore walls are quite thin and are comprised of a few individual flakes. When KOH or LiOH solutions were used instead, there were no apparent differences in the final 3D networks obtained (compare Fig. 3a and Fig. S5). Fig. S6a plots the nitrogen gas, N_2, isotherms of the Na-*c*-$Ti_3C_2T_x$ flakes, that exhibit distinct hysteresis loops in the range of

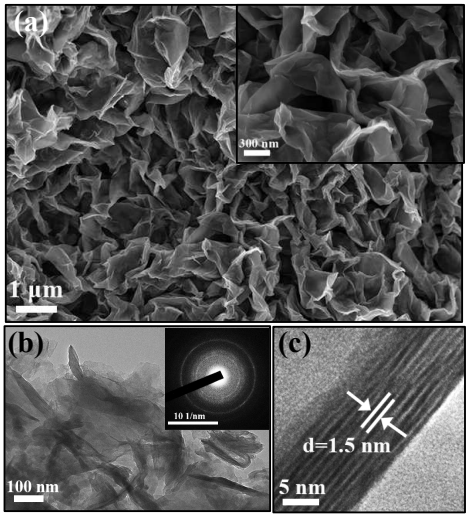

Fig. 3 (a) SEM images of Na-*c*-$Ti_3C_2T_x$ flocculated networks. Inset shows a higher magnification image. (b) TEM image. Inset shows SAED pattern of same region. (c) Higher magnification TEM image showing stacked layers.

0.5−1.0 P/P_0. Just as the corresponding pore size distributions (inset in Fig. S6a), there are spikes around 4 nm, 20 nm and 60 nm, suggesting the presence of a hierarchically porous structure. The BET surface area of the Na-*c*-$Ti_3C_2T_x$ was to be 21.4 m^2 g^{-1} This value is not significantly different than the values obtained for accordion-like MXene multilayers obtained after etching by HF.[19,20] The BET surface areas of the K-*c*-$Ti_3C_2T_x$ and Li-*c*-$Ti_3C_2T_x$, powders were measured to be 40 and 71 m^2 g^{-1}, respectively (Fig. S6b and c).

Fig. 3b shows TEM images of flocculated Na-*c*-$Ti_3C_2T_x$. Here again, the crumpled structures have many wrinkles and folds, as well as, many irregular pores. The selected-area electron diffraction pattern (SAED), (inset in Fig. 3b), was obtained with the electron beam parallel to <0001>. The *a* lattice parameter is calculated to be 0.317±0.007 nm, which is in good agreement with the corresponding value in the parent MAX phase. The higher magnification TEM images (Fig. 3c), show that the number of restacked nanosheets in the walls is of the order of 10. Applying the Scherrer formula to the most intense basal (0002) peaks in Fig. 2, yields values of ≈ 13 nm for the average thickness of the particle dimension along [0001]. This is an important result since it confirms that the number of individual MXene layers in the walls, between pores, is of the order of 10-15. This was further confirmed by atomic force microscopy (Fig. S7), where the thickness of a ML particle was measured to be ≈ 2 nm. Lastly, at ≈ 15 Å, the basal spacing between the layers obtained from the TEM image in Fig. 3c, is consistent with the 15.6 Å value calculated from the XRD results (Fig. 2).

In the remainder of this paper we present electrochemical measurements to demonstrate that the performance of our M'-*c*-$Ti_3C_2T_x$ powders in a Na-ion cell is better than either MLs or filtered films. Fig. S8a shows cyclic voltammetry (CV) scans of a Na-*c*-$Ti_3C_2T_x$ electrode measured at 0.2 mV s^{-1}. The cathodic peak, observed at 1.0 V during the first sodiation cycle, corresponds to the intercalation of Na^+ ions. The increased negative current below 1.0 V in the first sodiation cycle suggests the formation of a solid electrolyte interphase (SEI) film caused by electrolyte decomposition or other irreversible reactions.[21] From the second cycle on, this peak shifts to a lower voltage of ≈ 0.62 V, which is lower than that previously reported for $Ti_3C_2T_x$ materials, such as 1.1 V for alkalized $Ti_3C_2T_x$.[22] Fig. 4a shows discharge/charge curves in the voltage range of 0.01 – 3.0 V, at a current density of 25 mA g^{-1}. In the first cycle, the Na-*c*-$Ti_3C_2T_x$ electrode exhibited a discharge capacity of 267 mAh g^{-1}. In the second cycle, the capacity dropped to 170 mAh g^{-1} and continued to slowly decrease with further cycling. Note that the galvanostatic discharge/charge curves do not display a plateau region, indicating that the charge storage mechanism is most probably capacitive.[23] Moreover, after ten cycles, the charge-discharge curves were reproducible indicating better reversibility of the electrode/ion interaction processes.

Fig. S8b shows the specific capacity of three cells with different $Ti_3C_2T_x$ electrodes – 3D Na-*c*-$Ti_3C_2T_x$, MLs and a filtered film –all cycled at 100 mA g^{-1} for 500 cycles. The worst performing electrode was the filtered film, and the best was the 3D Na-*c*-$Ti_3C_2T_x$, which demonstrated outstanding cycling stability and maintained a capacity of 130 mAh g^{-1} after 500 cycles. The average discharge capacities of our Na-*c*-$Ti_3C_2T_x$ electrode were calculated to be 172.5, 148.3, 130.4, 108.7, 87.5, 68.8 and 61 mAh g^{-1} at current densities of 25, 50, 100, 200, 400, 800 and 1000 mA g^{-1}, respectively (Fig. S8c). The specific capacity increased back to 170.5 mAh g^{-1} when the current density

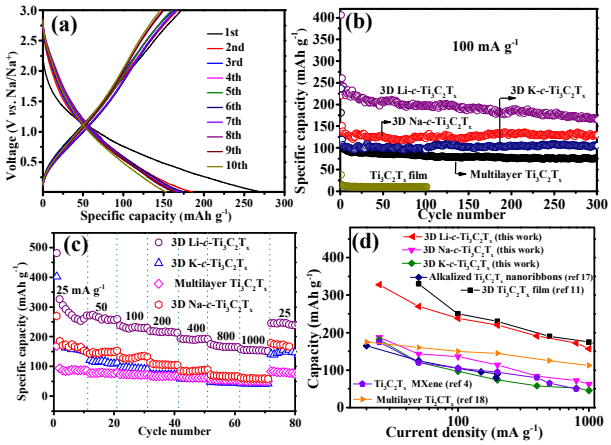

Fig. 4 Electrochemical characterization of electrodes in Na-ion cells: (a) Discharge/charge curves of Na-*c*-$Ti_3C_2T_x$ at a current density of 25 mA g^{-1}. (b) Cycling comparison at a current density of 100 mA g^{-1}. (c) Rate performance comparison at different current densities. (d) Comparison of the capacity achieved by the different *c*-$Ti_3C_2T_x$ electrodes with other reported pure MXene materials used in SIBs.

was reduced to 25 mA g^{-1}, indicating the ability of the crumpled MXene electrodes to tolerate higher currents. That cycling performance at higher currents is even better demonstrated by the results shown in Fig. S9, where a capacity of 54 mAh g^{-1} was maintained at a current density of 1.5 A g^{-1} for 1000 cycles. The excellent capacity retention can be attributed in part to the pillaring effect of the fraction of electrochemically inactive cations and the water molecules pre-trapped between the expanded $Ti_3C_2T_x$ layers, suppressing expansion/contraction of the interlayer spacing caused by reversible electrochemical ion cycling.[18,21,24]

Two results stand out here. The relatively low – for MXenes - first cycle irreversibility and the excellent cycling performance. Elemental mapping of Na-*c*-$Ti_3C_2T_x$ confirmed the homogeneous distribution of Ti, C, and Na (Fig. S10a). Energy-dispersive X-ray spectroscopy (EDS) spectrum of Na-*c*-$Ti_3C_2T_x$ (Fig. S10b), which shows that the sample consists of Ti, C, Na, as well as other surface terminations elements (O, Cl and F). The Na atomic ratio was ≈ 3% (Table S2). In general, the alkali content was quite low in the electrodes studied. Their small concentration is thus not believed to affect the measured capacities compared to the Na ions intercalated during the first cycle. That is not to imply that the role of pre-intercalated alkali ions is unimportant, however. Large irreversible losses during the first cycle are more often than not encountered when MXenes electrodes are tested.[4] Here, the capacity loss, from the first to the second cycle is about 36% (Fig. 4a). As far as we are aware, this value is the best ever reported for a MXene-based Na electrode. It is better than the 53.8%, 66 % or 44% values reported by Zhao et al.[11] Xie et al.[9] or Wang et al.[4] respectively. Said otherwise, pre-sodiation, that occurs during the crumpling process when NaOH is used, appears to mitigate irreversible cationic losses in the first cycle. This conclusion is further bolstered by our recent work on $Ti_3C_2T_x$ flakes crumpled using HCl and other common acids. At ~ 600 mAh g^{-1}, the irreversible first discharge capacities, on cells almost identical to those tested here, were more than double the ones reported herein.[12]

The main aim of this paper was to report on a facile, rapid technique to create mesoporous MXene microstructures. The second aim was to show that the latter is better suited as a Na-ion electrode material than ML-particles of the same composition. Up to this point, the focus has been on Na-*c*-$Ti_3C_2T_x$. Our underlying assumption was that a Na-containing electrode would be the most suited. Towards the end of the study, however, we wanted to show that other cations can be used as well. Figs. 4b and 4c compare the electrochemical performances of K-*c*-$Ti_3C_2T_x$, Li-*c*-$Ti_3C_2T_x$, and Na-*c*-$Ti_3C_2T_x$ electrodes. Somewhat surprisingly, the Li-*c*-$Ti_3C_2T_x$-based anode exhibited the best performance by a substantial margin. At 0.1 A g^{-1}, the capacity was ≈ 160 mAh g^{-1} after 300 cycles (Fig. 4b).

At this time the reason why the Li-containing electrodes were the best is unclear. On the one hand, it is tempting to ascribe the differences to the smaller ionic radius of Li. This phenomenon was observed in previous work, where we showed that smaller ionic radii showed better performance.[25] And while that may be correct here, it is worth noting that when the $d_{c/2}$ spacings are compared (Fig. 2), it is clear that the cations are surrounded by a robust water hydration shell and thus cationic size alone does not tell the entire tale.[13] Along the same lines it is important to note that while the $d_{c/2}$ values may well be important initially, cycling greatly increases that value due to the penetration of the electrolyte between layers.[12, 21] In other words, in this work the initial $d_{c/2}$ may not be critical in determining the long term capacities. The same can be said of the BET values. In MXenes, as opposed to carbon electrodes, the capacities are not strongly correlated with BET surface areas because the gases used in measuring the surface area do not penetrate between the MLs.

In short more work is needed before the discoveries made here are better understood. Lastly, Fig. 4d plots the capacity results reported to date for MXene electrodes devoid of spacers such as C nanotubes or other nanoparticles.[4,11,17,18] Based on these results and Table S3, it is clear that our electrodes based on Li-*c*-$Ti_3C_2T_x$, compare quite well with some of the highest values reported in the literatures.[4,11,17,18,21-23]

In conclusion, we show that the addition of LiOH, NaOH, KOH or TBAOH to $Ti_3C_2T_x$ colloidal suspensions results in the crumpling of the 2D flakes and flocculation into a 3D porous, foam-like network. The size of the macropores is around 300 nm and the size of the mesopores is ≈ 4 nm. Comprised of ≈ 15 individual flakes, the MXene walls between the pores are quite thin. Meanwhile, the 3D framework can be used as a high-performance Na-ion battery electrode. Respectable capacity values (165 mAh g^{-1} at 25 mA g^{-1} and 126 mAh g^{-1} at 100 mA g^{-1}) and long-term stability of over 500 cycles at a rate of 100 mA g^{-1} and even 1500 mA g^{-1} are achieved. Significantly better values are possible when the crumpling is carried out with LiOH, as compared to KOH or NaOH.

The main goal of this work was not to optimize the electrodes' architectures to maximize the power and energy densities, but rather to use electrochemistry to show that our 3D porous architecture was indeed different/better than ML particles or filtered films. This comment notwithstanding, and to our pleasant surprise, the electrochemical characteristics obtained for our un-optimized electrodes were quite respectable, especially in the Li-*c*-$Ti_3C_2T_x$ case. These results are encouraging enough that we are currently trying to optimize our fabrication methods to further enhance the electrochemical performances for Na and other cations. Like in the case of the use of $Ti_3C_2T_x$ for supercapacitors, for example, where the capacitance values increased from 300 F/cm^3 in 2013[16] to over 1400 F/cm^3 most recently.[26] it is reasonable to assume that rapid progress in the use of crumpled MXene is imminent and achievable.

Returning to the main aim of this work: Here we present a new method for designing 3D porous MXene-based materials that can be used in fields other than electrochemistry, such as catalysis, environmental, and biomedical applications. Most importantly, the facility and ease, by which we form our crumpled architecture should prove, in the long term, to be of great technological import.

ACKNOWLEDGMENTS

This work was supported by the Swedish Research Council under Grant No. 621-2014-4890. It was also partially supported by the National Natural Science Foundation of China (Nos. 21471016). EP and MC thank the support from the National Science Foundation (Grant No. DMR-1609272). We thank the Drexel Core Facilities and staff for assistance with characterization involving XRD, SEM and TEM. D.Z. was supported by the Chinese Scholarship Council.

Notes and references

1 M. W. Barsoum, M. Radovic, Annu. Rev. Mater. Sci. *Annu. Rev. Mater. Sci.* 2011, **41**, 195-227.
2 M. Naguib, M. Kurtoglu, V. Presser, J. Lu, J. Niu, M. Heon, L. Hultman, Y. Gogotsi, and M. W. Barsoum, *Adv. Mater.*, 2011，**23**，4248–4253.
3 M. Ghidiu, M. R. Lukatskaya, M. Q. Zhao, Y. Gogotsi, M. W. Barsoum, *Nature,* 2014, **516**, 78-81.
4 X. Wang, X. Shen, Y. Gao, Z. Wang, R. Yu, L. Chen, *J. Am. Chem. Soc.,* 2015, **137**, 2715-2721.
5 L. Ding, Y. Wei, Y. Wang, H. Chen, J. Caro, H. Wang, *Angew. Chem. Int. Ed.,* 2017, **56**, 1825-1829.
6 T. Y. Ma, J. L. Cao, J. Mietek, S. Z. Qiao, *Angew. Chem. Int. Ed.,* 2016, **55**, 1138-1142.
7 B. Xu, M. Zhu, W. Zhang, X. Zhen, Z. Pei, Q. Xue, C. Zhi, P. Shi, *Adv. Mater.,* 2016, **28**, 3333-3339.
8 B. Anasori, M. R. Lukatskaya, Y. Gogotsi, *Nat. Rev. Mater.,* 2017, **2**, 16098.
9 X. Xie, M. Q. Zhao, B. Anasori, K. Maleski, C. E. Ren, J. Li, B. W. Byles, E. Pomerantseva, G. Wang, Y. Gogotsi, *Nano Energy,* 2016, **26**, 513-523.
10 S. A. Shah, T. Habib, H. Gao, P. Gao, W. Sun, M. J. Green, M. Radovic, *Chem. Commun.,* 2016, **53**, 400-403.
11 M. Q. Zhao, X. Xie, C. E. Ren, T. Makaryan, B. Anasori, G. Wang, Y. Gogotsi, *Adv. Mater.,* 2017, **29**,1702410.
12 V. Natu, M. Clites, E. Pomerantseva, M. W. Barsoum, *Mater. Res. Lett.*, 2018, **6**, 230-235.
13 M. Ghidiu, J. Halim, S. Kota, D. Bish, Y. Gogotsi, M. W. Barsoum, *Chem. Mater.,* 2016, **28**, 3507-3514.
14 J. M. Luo, W. K. Zhang, H. D. Yuan, C. B. Jin, L. Y. Zhang, H. Huang, C. Liang, Y. Xia, J. Zhang, Y. P. Gan, X. Y. Tao, *ACS Nano*, 2017, **11**, 2459−2469.
15 M. Ghidiu, M. W. Barsoum, *J. Amer Ceram Soc*., 2017, **100**, 5395-5399.
16 M. R. Lukatskaya, O. Mashtalir, C. Ren, Y. Dall'Agnese, P. Rozier, P. L. Taberna, M. Naguib, P. Simon, M. B. Barsoum, Y. Gogotsi, *Science,*2013, **341**, 1502-1505.
17 P. Lian, Y. Dong, Z. S. Wu, S. Zheng, X. Wang, W. Sen, C. Sun, J. Qin, X. Shi, X. Bao, *Nano Energy,* 2017, **40**, 1-8.
18 X. Wang, S. Kajiyama, H. Iinuma, E. Hosono, S. Oro, I. Moriguchi, M. Okubo, A. Yamada, *Nat. Commun.,* 2015, **6**, 6544.
19 R. B. Rakhi, B. Ahmed, M. N. Hedhili, D. H. Anjum, H. N. Alshareef, *Chem. Mater.,* 2015, **27**, 5314-5323.
20 A. K. Fard, G. McKay, R. Chamoun, T. Rhadfi, H. Preud'Homme, M. A. Atieh, *Chem. Eng. J.,* 2017, **317**, 331-342.
21 S. Kajiyama, L. Szabova, K. Sodeyama, H. Iinuma, R. Morita, K. Gotoh, Y. Tateyama, M. Okubo, A. Yamada, *ACS Nano,* 2016, **10**, 3334-3341.
22 Y. Xie, Y. Dall'Agnese, M. Naguib, Y. Gogotsi, M. W. Barsoum, H. L. Zhuang, P. R. C. Kent, *ACS Nano,* 2014, **8**, 9606-9615.
23 Y. Dall'Agnese, P. L. Taberna, Y. Gogotsi, P. Simon, *J. Phys. Chem. Lett.,* 2015, **6**, 2305-2309.
24 M. Clites, B. W. Byles, E. Pomerantseva, *J. Mater. Chem. A,* 2016, **4**, 7754-7761.
25 M. Clites, E. Pomerantseva, *Energy Storage Materials*, 2018, **11**, 30-37.
26 M. R. Lukatskaya, S. Kota, Z. Lin, M. Q. Zhao, N. Shpigel, M. D. Levi, J. Halim, P. L. Taberna, M. W. Barsoum, P. Simon, Y. Gogotsi, *Nature Energy,* 2017, **6**, 17105.